Influence of Activation Method on Coconut-Shell-Derived Carbon Supports for Ni and Ni–Ce Catalysts in CO2 Methanation

energy&fuels

pubs.acs.org/EF
Article

Influence of Activation Method on Coconut-Shell-Derived Carbon Supports for Ni and Ni–Ce Catalysts in CO_2 Methanation

Published as part of Energy & Fuels special issue "Celebrating Authors of Energy and Fuels Most-impactful Articles (2023)".

Vittorio Vitacchione, Paula Teixeira, José M. Lopes, Carlos Henriques, Stefania Specchia,* and Carmen Bacariza*

Cite This: *Energy Fuels* 2026, 40, 14787–14798

ABSTRACT: Three activated carbons derived from coconut shell were investigated as catalyst supports, each prepared using a different activation method: physical activation with CO_2 and chemical activation with H_3PO_4 and $ZnCl_2$. Ni and Ni–Ce catalysts were synthesized via incipient wetness impregnation and co-impregnation, respectively, and characterized using ICP analysis, N_2 adsorption, TGA, SEM-EDX, and TEM. Prior to catalytic evaluation, the materials were assessed in terms of hydrophobicity, textural properties (pore volumes, surface areas), and metal dispersion. Catalytic performance was tested under both conventional and aging conditions at atmospheric pressure over a temperature range of 240–450 °C (GHSV = 86100 mL h^{-1} g_{cat}^{-1}, H_2:CO_2 = 4:1). The activation method was found to strongly influence the structural properties of the supports. In particular, CO_2 activation produced a predominantly microporous carbon, whereas chemically activated carbons exhibited different pore structures and contained residual species from the activating agents. Among the Ni-based catalysts, the one supported on CO_2-activated carbon showed the best performance, attributed to its higher basicity, measured by the determination of the pH_{PZC}. The incorporation of Ce further enhanced catalytic activity by improving Ni dispersion and promoting CO_2 activation on CeO_2 sites. Overall, the highest CH_4 yield (~80% at 370 °C) was achieved with catalysts containing 20 wt % Ni and 20 wt % Ce supported on H_3PO_4 and CO_2-activated carbons. The CO_2-activated support was identified as the most promising due to its greener preparation route and superior performance, maintaining stable activity under aging tests without significant deactivation.

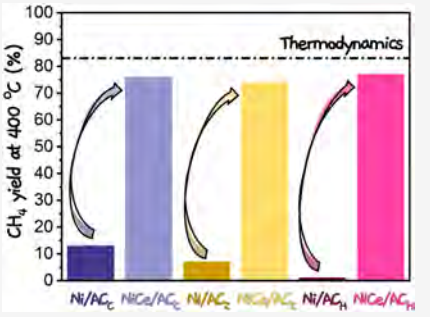

1. INTRODUCTION

Power-to-Gas (PtG) technology offers a highly effective solution for energy storage and carbon mitigation, with CO_2 methanation (Sabatier reaction, eq 1) playing a crucial role. This process involves reacting hydrogen (H_2), generated through water electrolysis using renewable electricity, with carbon dioxide (CO_2) sourced from industrial emissions, surplus biogas plant emissions, or carbon capture and storage (CCS) systems. The resulting synthetic natural gas (SNG) seamlessly integrates into existing gas infrastructure, enhancing renewable energy utilization while significantly reducing greenhouse gas (GHG) emissions.

$$CO_2 + 4H_2 \rightarrow CH_4 + 2H_2O \quad \Delta H_{298K} = -165\ \text{kJ/mol} \tag{1}$$

Given the high stability of carbon dioxide, CO_2 methanation requires the use of catalysts. Literature works have mainly focused on the use of transition (Ni, Co, Fe)[1,2] and platinum-group (Ru, Rh)[3,4] metals, supported on porous materials such as zeolites[5] or on oxide supports such as Al_2O_3, CeO_2, ZrO_2, and La_2O_3.[6−10] Among the active metals, Ni-based catalysts are known to provide an optimal balance of activity, selectivity, and cost-effectiveness;[10] however, they are prone to deactivation due to carbon deposition, sintering, or agglomeration at high temperatures.[11,12] In terms of supports, although oxide supports are widely used, they can suffer from limited low-temperature performance, insufficient CO_2 activation, and catalyst deactivation through sintering or unfavorable metal–support interactions.[6−10] These limitations motivate the search for alternative supports combining high surface area, chemical stability, tunable surface chemistry, and strong metal–support interactions. Carbon-based supports are therefore an attractive alternative, particularly activated carbons derived from biomass and biowastes, because they

Received: April 1, 2026
Revised: June 18, 2026
Accepted: June 19, 2026
Published: June 26, 2026

https://doi.org/10.1021/acs.energyfuels.6c01629
Energy Fuels 2026, 40, 14787–14798

combine a high surface area, thermal stability, and low cost with sustainable feedstock availability.

The use of carbon materials as catalyst supports has gained significant attention.[13,14] Regarding their application in CO_2 methanation,[15−17] their high surface area has been reported to provide binding sites that stabilize metal nanoparticles, prevent sintering, and enhance catalytic performance. Additionally, they have been pointed out as highly resistant to carbon deposition.[15,16] Their high surface-to-volume ratio has been reported to improve access to active sites and mass transfer of reactants and products, while their enhanced basicity further improves CO_2 adsorption,[18] boosting methanation performance at lower temperatures. Among carbon-based supports, activated carbon (AC)-supported catalysts are particularly attractive from an environmental point of view, as ACs can be prepared from biomass or biowaste (e.g., cork, olive stones, lignin) by physical and chemical activation methods,[19] making them a sustainable and eco-friendly choice for CO_2 capture[20] and CO_2 methanation.[15]

AC-supported catalysts containing transition metals (Co, Cu, and Ni) have been explored by Ha et al.[21] using theoretical methods, including Monte Carlo simulations, density-functional theory (DFT), and molecular dynamics (MD). Ni/AC and Co/AC were shown to be the most effective systems for the chemical adsorption of CO_2, demonstrating strong activity for CO_2 methanation owing to the AC's high surface area and pore volume, which allows it to store both H_2 and CO_2 (reservoir effect).[21,22] Despite the ability of ACs to adsorb and/or accommodate CO_2 molecules within their porous structure, the enhancement of their CO_2 adsorption capacity through the incorporation of promoters such as Ce, Mg, Mo, Ca, Cr, Mn, Cu, Fe, Zn, Ru, and Ga oxides[23,24] or nitrogen-containing functional groups[16,25,26] has been widely explored. Among the metal oxides, Gonçalves et al.[27] synthesized a composite support of cork-derived activated carbon and CeO_2 ($AC-CeO_2$), along with pure CeO_2, and deposited Ni nanoparticles via incipient wetness impregnation. The authors found that the optimal temperature for CO_2 methanation was reduced by 80 °C compared to a CeO_2-free Ni/AC catalyst. In situ modulation-excitation phase-sensitive detection DRIFTS (ME−PSD−DRIFTS) revealed that methanation over Ni/CeO_2 involved both CO and formate pathways, while over Ni/$AC-CeO_2$ it occurred exclusively via the formate pathway, producing CH_4 without intermediate CO formation. Regarding the comparison of metal oxides and nitrogen-containing functional groups, Di Stasi et al.[28] evaluated the CO_2 conversion and CH_4 selectivity of a wheat straw activated carbon loaded with ceria or urea as promoters alongside nickel as the active phase. The authors found that while urea doping introduced nitrogen-containing functionalities onto the activated carbon surface, the improvement in catalytic activity was modest compared to the significant enhancement achieved with ceria as a promoter.

Despite the growing number of publications on AC-supported catalysts for CO_2 methanation, a critical gap persists in the literature regarding the systematic evaluation of the influence of the AC preparation method on catalytic performance when the raw material is held constant. Reviews and bibliometric analyses have acknowledged that AC porosity and surface chemistry can be profoundly tuned through preparation conditions and that these properties govern metal dispersion and ultimately catalytic performance,[15] yet the vast majority of studies compare catalysts supported on ACs derived from different precursors or commercially sourced carbons.[16] A dedicated CO_2 methanation study comparing the properties and performance of metal-based catalysts supported on ACs synthesized by different methods using the same biomass residue precursor has not yet been reported.

This work explores the use of coconut shells as a sustainable activated carbon precursor, evaluating the influence of the preparation method on the properties and performance of the resulting metal-loaded catalysts. Three preparation routes were selected to cover a broad range of activation strategies:[19,29−32] CO_2 physical activation, which yields carbons with well-developed microporosity and minimal surface contamination; chemical activation with H_3PO_4, which promotes mesopore development and may introduce phosphorus-containing surface groups; and chemical activation with $ZnCl_2$, which produces carbons with distinct pore size distributions and surface chemistries. This comparative approach allows the effect of the activation method on metal dispersion, hydrophobicity, and ultimately catalytic performance to be systematically assessed. Ni and Ce were incorporated onto the synthesized supports by incipient wetness impregnation, and the resulting materials were characterized by a range of advanced techniques and tested in the Sabatier reaction. By evaluating how the activation method influences the physicochemical properties and catalytic performance of the catalysts, this work provides valuable insights into the Sabatier reaction over activated carbons.

2. EXPERIMENTAL SECTION

2.1. Catalysts Synthesis

2.1.1. Activated Carbons' Preparation. Three activated carbons prepared using coconut shell residues from Brazil as starting material were provided by *Faculdade de Ciências e Tecnologia* of the *Universidade Nova de Lisboa*. Dried coconut shells were ground and sieved to obtain a particle size between 1 and 3 mm. Two activated carbons were obtained by chemical activation using phosphoric acid (H_3PO_4; AC_H) and zinc chloride ($ZnCl_2$; AC_Z). The particles were impregnated with the chemical agents using an impregnation mass ratio of 2.5 and kept at 80 °C for 4 h. Pyrolysis was then carried out for 3 h at 450 °C (H_3PO_4 activation) and 600 °C ($ZnCl_2$ activation) under a constant nitrogen flow of 83 mL min^{-1} (5 °C min^{-1}). After that, the chemically activated samples were washed with distilled water and dried at 105−110 °C for 24 h. The AC obtained using $ZnCl_2$ was previously washed with an HCl solution (2 N). The third AC (AC_C) was obtained by physical activation using CO_2. For this purpose, coconut shell particles were first carbonized for 4 h at 800 °C (2 °C min^{-1}) under a constant nitrogen flow (83 mL min^{-1}). After cooling down to room temperature, they were subsequently heated up to 800 °C (2 °C min^{-1}) under a CO_2 flow (17 mL min^{-1}), keeping this temperature for 4 h. Finally, the three ACs were ground and sieved to obtain a particle size below 150 μm. The main synthesis steps followed for synthesizing these materials are summarized in Table 1.

2.1.2. Ni and Ni−CeO_2 Catalysts' Preparation. After support synthesis, Ni and Ni−CeO_2 catalysts were prepared by incipient wetness impregnation and coimpregnation, respectively, using nickel nitrate hexahydrate ($Ni(NO_3)_2{\cdot}6H_2O$, 98.5% purity) and cerium nitrate hexahydrate ($Ce(NO_3)_3{\cdot}6H_2O$, 99% purity) from Sigma-Aldrich as precursors, and 2-propanol (Scharlau, analytical grade) as the impregnation solvent. After impregnation, the samples were dried overnight at 80 °C and thermally treated at 500 °C (1 h, 2 °C min^{-1}) under nitrogen flow (120 mL min^{-1} g^{-1}). After a preliminary study carried out on AC_H to select the most appropriate Ni loading testing contents from 2 to 20 wt %, the catalysts listed in Table 2 were synthesized.

https://doi.org/10.1021/acs.energyfuels.6c01629
Energy Fuels 2026, 40, 14787−14798

Table 1. Preparation Conditions Used for the Activated Carbons Studied in This Work

Code	Synthesis steps
AC_H	Impregnation with H_3PO_4; drying at 80 °C (4 h); thermal treatment at 450 °C (3 h, N_2 flow); washing with distilled water; drying at 105−110 °C (24 h)
AC_Z	Impregnation with $ZnCl_2$; drying at 80 °C (4 h); thermal treatment at 600 °C (3 h, N_2 flow); washing with distilled HCl and distilled water; drying at 105−110 °C (24 h)
AC_C	Carbonization at 800 °C (4 h, N_2 flow); thermal treatment at 800 °C (4 h, CO_2 flow)

Table 2. Preparation Conditions Used for the AC-Supported Catalysts from This Work

Code	Method	Ni loading[a] (wt %)	Ce loading[a] (wt %)
Ni/AC_H	Incipient wetness impregnation with 2-propanol	20	-
Ni/AC_Z		22	-
Ni/AC_C		19	-
$NiCe/AC_H$	Incipient wetness coimpregnation with 2-propanol	21	21
$NiCe/AC_Z$		20	20
$NiCe/AC_C$		21	21

[a]Determined by ICP analysis.

2.2. Characterization Techniques

ICP analysis was performed for chemical analysis at the *Laboratório de Análises* of *Universidade de Aveiro*. The activated carbons' acid−base properties were assessed by determining the pH of zero charge (pH_{PZC}) at *Universidade Nova de Lisboa*. Powder XRD patterns were obtained using a Bruker AXS D8 Advance diffractometer with Cu Kα radiation, equipped with a 1D detector (SSD 160) and a Ni filter, scanning from 20° to 80° (2θ) with a step size of 0.03° and a step time of 0.5 s. N_2 sorption experiments were carried out on an Autosorb iQ instrument (Quantachrome) at −196 °C. ACs and catalysts (~70 mg) were degassed under vacuum at 110 °C for 7 h prior to analysis. Micropore volumes (V_{micro}) were derived from the t-plot method, total pore volumes (V_{total}) were measured at a relative pressure (p/p_0) of 0.95, and mesopore volumes (V_{meso}) were calculated as $V_{total} - V_{micro}$. Specific surface areas (S_{BET}) were determined by the BET method. Thermogravimetric analysis (TGA) was performed on a Setsys Evolution instrument (Setaram). Thermal decomposition of the activated carbons (AC_H, AC_Z, and AC_C) was assessed under N_2 and air atmospheres from 20 to 900 °C (heating rate: 10 °C min^{-1}) to evaluate their thermal stability and, in the air experiments, to quantify ash content. Ni and $Ni-CeO_2$ catalysts prepared on the three AC supports were additionally analyzed by TGA from 20 to 400 °C (heating rate: 10 °C min^{-1}) under N_2 flow after saturation with water vapor, to characterize their hydrophobic properties. The hydrophobicity index (h) was calculated as the ratio of mass loss at 150 °C to mass loss at 400 °C, following the methodology applied in our previous studies on zeolite-based catalysts.[33,34] SEM-EDS and TEM analyses were performed at *MicroLab* (*Instituto Superior Técnico, Universidade de Lisboa*). EDS analysis was carried out to determine the surface chemical states of the catalysts. Average Ni^0 particle sizes were determined from TEM micrographs using ImageJ software, with a minimum of 500 particles measured per sample. Metallic dispersions were estimated as reported elsewhere.[35]

2.3. Catalytic Tests

Catalytic performances were assessed by carrying out tests up to 450 °C, at atmospheric pressure, using a fixed-bed Pyrex reactor and 0.200 g of catalyst in powder form. The gases used were supplied by Air Liquide (purity ≥99.9990%), and their flows were controlled by mass-flow controllers from Brooks. A mixture of H_2, CO_2 and N_2 (molar ratio H_2:CO_2:N_2 = 36:9:10, total flow 287 mL min^{-1}) was fed to the reactor. The reactor effluent was diluted with N_2 prior to analysis to bring all gas concentrations within the detector range. Effluent composition was then analyzed using Guardian NG infrared detectors (Edinburgh Sensors) for CO_2, CH_4, and CO (0−10 vol % range), which provide an accuracy of ±2% of full scale, corresponding to an absolute error of ±0.2 vol % per channel. The experimental conditions were chosen based on previous works,[36] ensuring that no external mass transfer limitations were relevant, thereby obtaining observed kinetics free of mass transfer effects in the CO_2 transformation. Outlet flows were measured at each temperature, since this reaction proceeds with a reduction in the number of moles. The corresponding CO_2, CH_4, and CO molar flows were determined ($F_{CO2,\ outlet}$, $F_{CO,\ outlet}$, and $F_{CH4,\ outlet}$, respectively) and the carbon balances (98 to 102%) confirmed that CO and CH_4 were the only carbon-containing products. CO_2 conversion, CH_4 selectivity and CH_4 yield were calculated as shown in eqs 2, 3 and 4, respectively. For each catalyst, at least two catalytic tests were run under the same conditions to assess intermediate precision. Based on these results, the experimental relative error was estimated to be 2%.

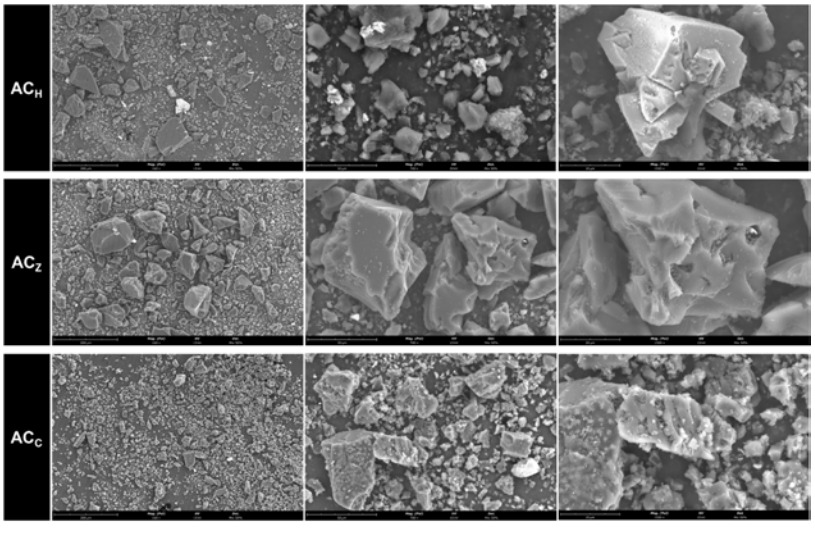

Figure 1. SEM micrographs collected for the three activated carbons at amplifications of 200, 50, and 20 μm.

https://doi.org/10.1021/acs.energyfuels.6c01629
Energy Fuels 2026, 40, 14787−14798

$$\text{CO}_2\ \text{conversion}\ (\%) = \frac{F_{CO_2,inlet} - F_{CO_2,outlet}}{F_{CO_2,inlet}} \cdot 100 \quad (2)$$

$$\text{CH}_4\ \text{selectivity}\ (\%) = \frac{F_{CH_4,outlet}}{F_{CO_2,inlet} - F_{CO_2,outlet}} \cdot 100 \quad (3)$$

$$\text{CH}_4\ \text{yield}\ (\%) = \frac{F_{CH_4,outlet}}{F_{CO_2,inlet}} \cdot 100 \quad (4)$$

For one of the best-performing catalysts, a longer test was also run to assess its stability over time and the robustness of the procedure. For this purpose, the following sequence of experiments at variable conditions was carried out for 9 days: (i) Day 1—test at variable temperatures (equivalent to that previously described); (ii) Days 2 to 6—test at ~350 °C for 30 h (6 h/day) under reaction conditions; (iii) Day 7—test at ~250 °C for 6 h under reaction conditions; (iv) Day 8—test at ~350 °C for 6 h under reaction conditions; and (v) Day 9—test at variable temperatures [same as (i)].

3. RESULTS AND DISCUSSION

3.1. Supports Characterization

Activated carbons were first characterized by SEM analysis, with results shown in Figure 1. As observed, the activation strategy affects the morphological properties of the obtained activated carbons, with larger particles generally found for the AC_Z support. In all cases, particles with an irregular shape were identified. The differences in texture and the observations of regions with a brighter EDS response motivated the analysis of the materials by SEM-EDS (Figure S1 and Figure 2), with the aim of identifying the presence of potential contaminants on their surface. As observed, some contaminants are present in both AC_H and AC_Z samples. Indeed, in the former, the presence of P with traces of Fe, Ni, Cr, and Ti is evident, while in the latter, Cl and Zn are clearly identified. This indicates that in both cases, the chemical agent was not fully removed from the carbons. Furthermore, for the H_3PO_4-treated sample, trace metals may arise from leaching of metals from the equipment used during the synthesis by the acid. On the contrary, only traces of elements typically present in the coconut shell residues[37,38] (e.g., K, Si, Na, Al) were found in the physically activated material (AC_C).

Furthermore, TGA analysis was performed for the three activated carbons under nitrogen (to predict the potential stability during the thermal treatment to be carried out after Ni and/or Ce incorporation and, potentially, under catalytic tests, performed under a $CO_2/H_2/N_2$ flow) and air (to quantify the percentage of ashes) atmospheres, with the results presented in Figure 3. Starting with the results collected under nitrogen atmosphere (Figure 3-left), all materials exhibit a first water desorption mass loss process at around 150 °C. Afterward, AC_H and AC_C show a considerably lower thermal stability, with relevant mass losses up to 95% systematically registered above ~500 °C. On the contrary, AC_Z presented a considerably higher stability (mass loss <20% at 900 °C). Overall, considering that the thermal treatment for Ni and/or Ce precursor salt decomposition is performed under nitrogen atmosphere at 500 °C and that AC_H and AC_C remain stable below this temperature under inert conditions (Figure 3-left), no relevant support losses can be expected during catalyst preparation. Indeed, to confirm this, TGA analyses were performed over nickel nitrate precursor salt and Ni/AC_H after nickel impregnation (prior to the thermal treatment at 500 °C under N_2 flow). Results (Figure S2) indicate that salt's

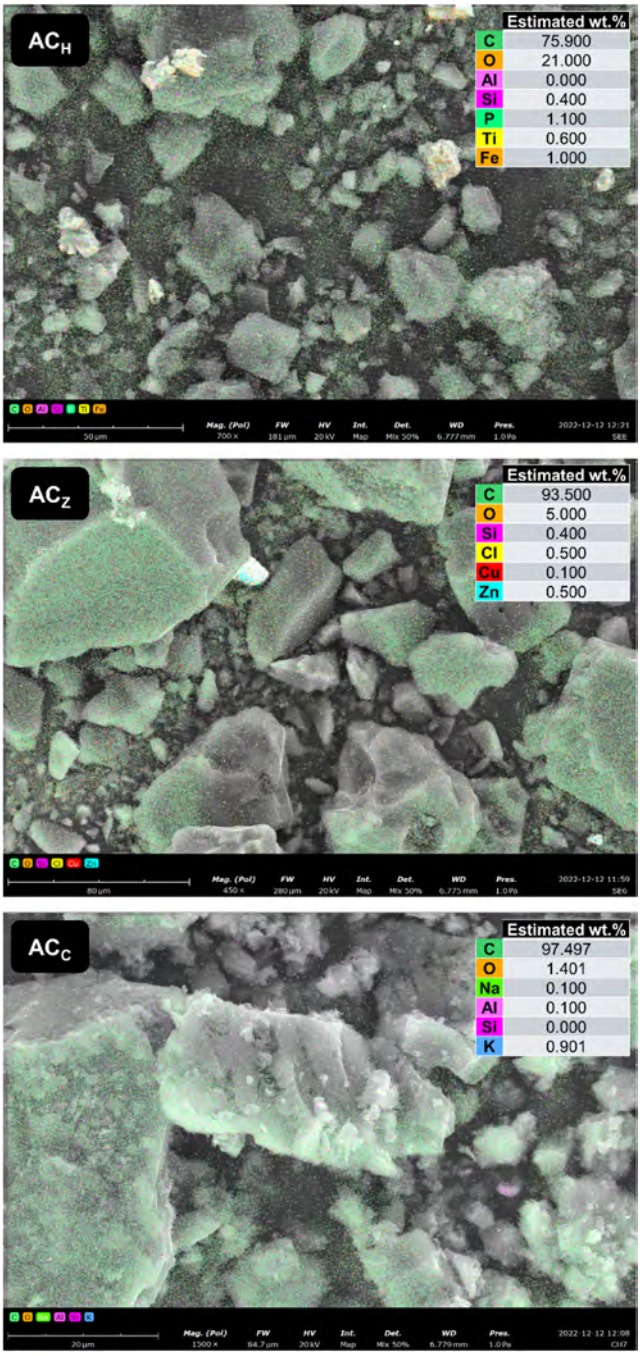

Figure 2. Mapping results collected for the three activated carbons.

decomposition is mostly completed at ~350 °C, being a similar decomposition process identified in the uncalcined Ni catalyst until ~500 °C. Considering that TGA is carried out under transient conditions (10 °C min^{-1}) and that the thermal treatment is performed at 500 °C for 1 h, the decomposition of the salt together with the preservation of the carbon can be expected during the thermal treatment. In addition, the proximity between the nominal and measured Ni and Ce loadings in the catalysts indicates that carbon decomposition is not relevant during the precursor salts' decomposition step. Regarding the experiments under air atmosphere to determine the ashes percentage (Figure 3-right), all carbons remain stable until ~500 °C, with significant mass losses registered above ~635 °C in all cases. These mass losses under oxidative

https://doi.org/10.1021/acs.energyfuels.6c01629
Energy Fuels 2026, 40, 14787−14798

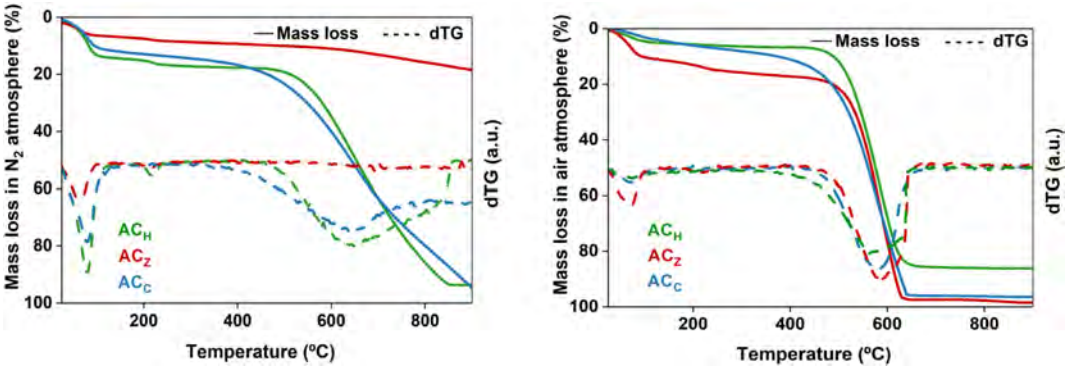

Figure 3. TGA results obtained for the activated carbons under nitrogen (left) and air (right) atmospheres.

conditions are ascribed to carbon oxidation, typically occurring between 550 and 700 °C,[39] and are not relevant to catalyst preparation or reaction conditions, which are conducted under inert or reducing atmospheres. While AC_Z and AC_C present <5% of ashes, the more remarkable presence of ashes in AC_H (~15%) could be ascribed to the greater presence of contaminants (e.g., Fe, Cr, Ni) in this carbon in accordance with previously discussed SEM-EDS results.

In terms of XRD data (Figure S3), the amorphous nature of the carbons was proven,[40] with additional peaks attributed to contaminants found in AC_H and AC_Z samples. For instance, the diffraction peaks located at 31.61°, 34.26°, 36.10°, 47.37°, 56.40°, 62.68°, and 67.72° correspond to the (100), (002), (101), (102), (110), (103), and (112) reflection planes of the hexagonal structure of the ZnO for AC_Z, the one treated with $ZnCl_2$.[41] N_2 sorption experiments were also conducted to assess the textural properties of the carbons (V_{micro}, V_{meso}, and S_{BET}) as well as to analyze the pore size distribution. While the isotherms and pore size distributions can be seen in Figure S4, the textural properties can be found in Table 3. As observed, all

Table 3. Textural and Basic Properties of the Activated Carbons

Sample	V_{micro} [a] ($cm^3\ g^{-1}$)	V_{meso} [b] ($cm^3\ g^{-1}$)	S_{BET} [c] ($m^2\ g^{-1}$)	pH_{PZC} [d]
AC_H	0.14	0.73	1285	2.4
AC_Z	0.10	0.70	1246	6.2
AC_C	0.16	0.06	473	9.7

[a]Total micropore volume was determined from N_2 sorption analysis using the *t-plot* method. [b]Mesopore volume was determined as $V_{total} - V_{micro}$. [c]Specific surface area was determined by the BET method. [d]pH Point of Zero Charge.

ACs present both micro- and mesoporous features, with the mesoporosity being promoted by chemical activation synthesis methods. Indeed, both AC_H and AC_Z present higher V_{meso} values (0.70–0.73 $cm^3\ g^{-1}$) than AC_C (0.06 $cm^3\ g^{-1}$). In terms of microporosity, even if the results are similar for the three carbons (0.10–0.16 $cm^3\ g^{-1}$), the highest value was achieved by the physically activated material. Regarding the BET surface areas (S_{BET}), once again similar results were obtained for the H_3PO_4 and $ZnCl_2$-treated materials (1285–1246 $m^2\ g^{-1}$), while a lower value was determined for AC_C, in accordance with its lower V_{meso}. Finally, pH_{PZC} values (Table 3) were used as indicators of the activated carbons' acidic-basic properties. As observed, the basicity, a favorable property for carbon dioxide activation, followed the order: $AC_C > AC_Z > AC_H$.

3.2. Metal-Based Catalysts' Characterization

After a prescreening of catalysts with variable Ni loadings over AC_H support (results presented in Figure S5 and Table S1), monometallic and bimetallic catalysts containing ~20 wt % Ni and ~20 wt % Ce were synthesized and characterized. Since H_2O is a product of CO_2 methanation and can competitively adsorb on the active sites, reducing the number of sites available for reactant interaction and thereby inhibiting reaction kinetics,[33,42,43] a hydrophobic support surface is desirable to limit water accumulation and improve catalytic efficiency. Hydrophobicity was therefore assessed by TGA through determination of the h index (Table 4). Values close

Table 4. Main Properties of the Ni and Ni–CeO_2-Based ACs

Sample	h index[a]	V_{micro} [b] ($cm^3\ g^{-1}$)	V_{meso} [c] ($cm^3\ g^{-1}$)	S_{BET} [d] ($m^2\ g^{-1}$)	ØNi^0 [e] (nm)	D [e] (%)
Ni/AC_H	0.95	0.16	0.29	763	21	4
$NiCe/AC_H$	0.91	0.04	0.17	281	7	13
Ni/AC_Z	0.99	0.14	0.40	902	24	4
$NiCe/AC_Z$	0.82	0.07	0.26	487	13	7
Ni/AC_C	1.00	0.19	0.06	531	16	5
$NiCe/AC_C$	0.91	0.10	0.12	322	8	11

[a]Hydrophobicity index was determined by TGA. [b]Total micropore volume was determined from N_2 sorption analysis using the *t-plot* method. [c]Mesopore volume was determined as $V_{total} - V_{micro}$. [d]Specific surface area was determined by the BET method. [e]Average Ni^0 particle size and metallic dispersion were obtained by TEM.

to 1 were obtained for all monometallic Ni-based catalysts, indicating that water interacts weakly with their surfaces, with most adsorbed water desorbed at 150 °C. The incorporation of cerium led, as previously observed in the literature,[36] to a slight reduction in hydrophobicity, ascribed to the favorable interaction of CeO_2 with water molecules.

As done for the supports, the structural characterization was assessed by XRD, with the patterns of fresh Ni/ACs and NiCe/ACs being presented in Figure 4A and Figure 4C, respectively. As observed, all catalysts exhibited the characteristic diffraction peaks of Ni^0 phases at ~45°, ~52°, and ~76°. In addition, CeO_2 phase peaks could be observed in NiCe/ACs at ~27°, ~33°, ~47°, and ~57°.

The catalysts' textural properties (V_{micro}, V_{meso}, and S_{BET}, Table 4) were obtained by the collection of N_2 isotherms (Figure 5). The results evidenced a stronger impact of Ni

https://doi.org/10.1021/acs.energyfuels.6c01629
Energy Fuels 2026, 40, 14787–14798

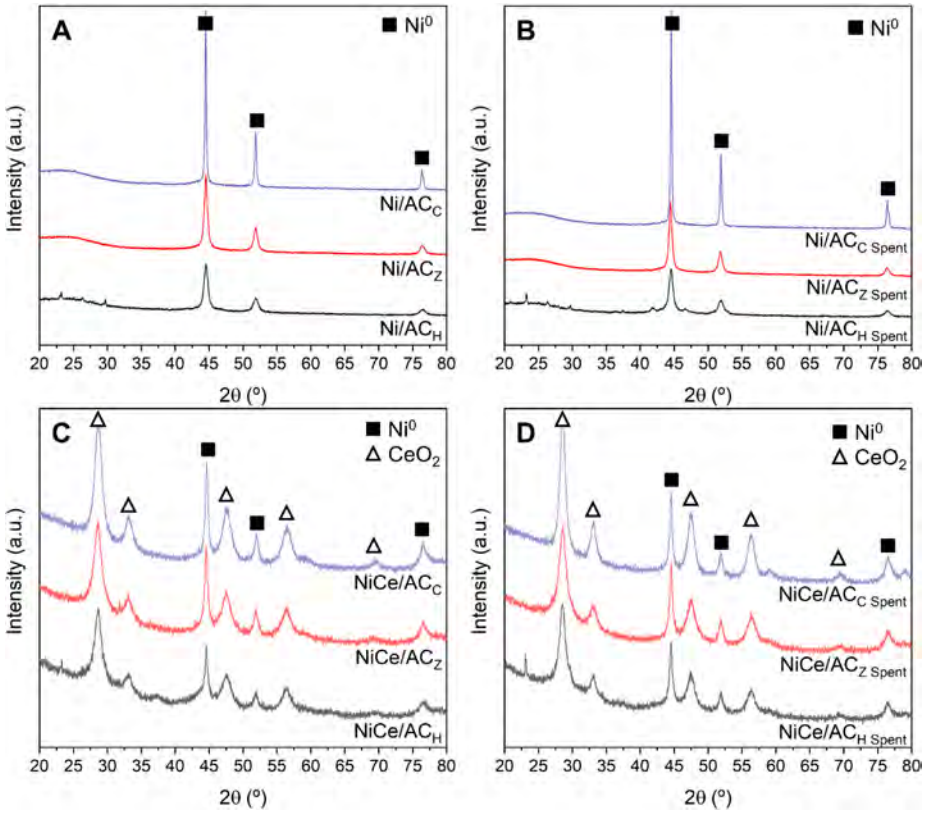

Figure 4. XRD patterns collected for Ni and Ni−CeO_2-based AC catalysts after synthesis (A−C, left) and catalytic tests (B−D, right).

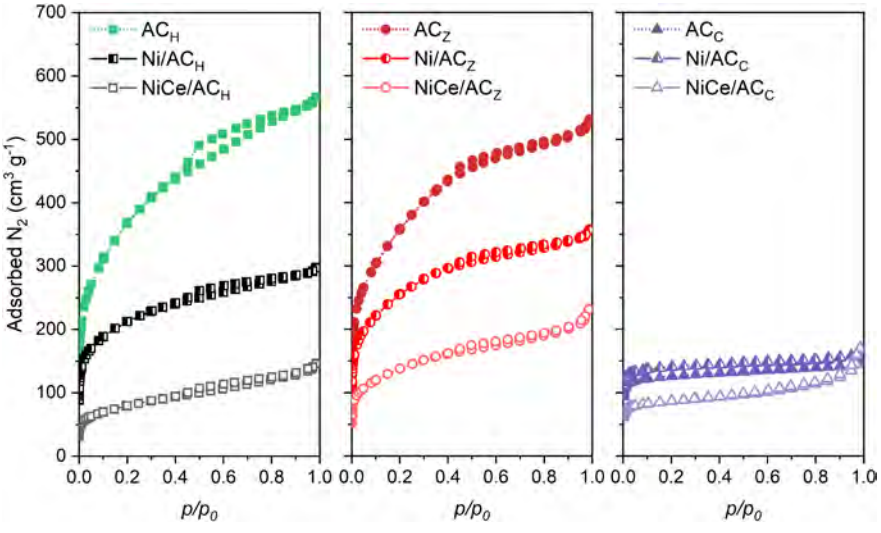

Figure 5. N_2 isotherms collected for Ni and Ni−CeO_2-based ACs as well as for the corresponding supports.

incorporation in the activated carbons synthesized by chemical activation (AC_H and AC_Z), which is manifested by a reduction of the mesoporous volumes and BET surface areas, respectively, from 0.70−0.73 $cm^3\ g^{-1}$ and 1246−1285 $m^2\ g^{-1}$ (AC_H and AC_Z, Table 2) to 0.29−0.40 $cm^3\ g^{-1}$ and 763−902 $m^2\ g^{-1}$ (Ni/AC_H and Ni/AC_Z, Table 4). This impact on the textural properties was considerably lower in AC_C, where V_{meso} and S_{BET} values of 0.06 $cm^3\ g^{-1}$ and ∼500 $m^2\ g^{-1}$ were obtained, respectively, in both the support and the Ni-containing catalyst. In terms of CeO_2 addition, as expected, a general reduction of the textural properties (pore volumes, surface areas) was observed in all cases. The decrease in surface area and mesopore volume may be attributed to partial pore filling and/or blockage by Ni species located within the porous structure. Pore sizes were not affected by metal addition, as seen in Figure S6. The stronger impact of Ni and ceria addition on the chemically activated carbons could possibly be attributed to the formation of larger particles in these samples (to be confirmed by TEM analysis).

TEM micrographs of the bare AC supports can be found in Figure S7, while those collected for Ni/ACs and NiCe/ACs can be found in Figures 6 and 7, respectively. While in the unloaded activated carbons there is no clear presence of metal particles, results for the Ni- and NiCe-containing catalysts

https://doi.org/10.1021/acs.energyfuels.6c01629
Energy Fuels 2026, 40, 14787−14798

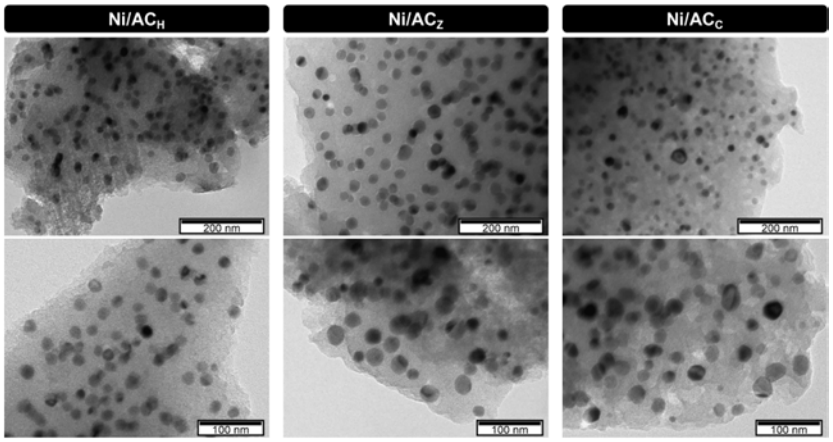

Figure 6. TEM micrographs obtained for Ni-based activated carbons.

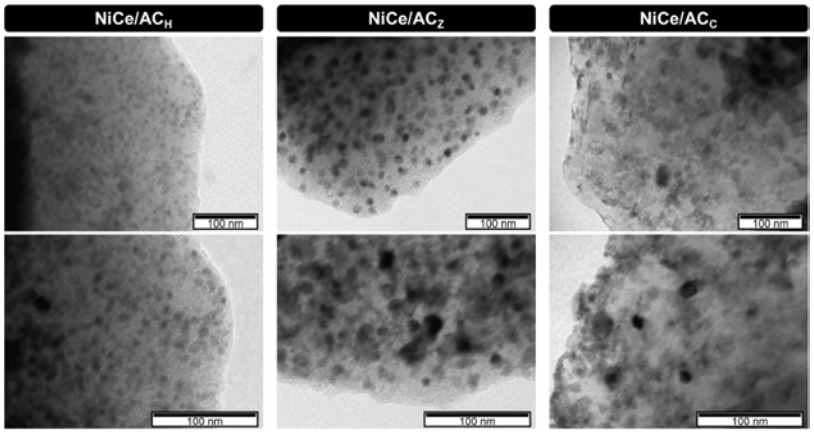

Figure 7. TEM micrographs obtained for Ni−CeO_2-based activated carbons.

allow the identification of well-dispersed metallic nickel particles, whose average sizes are presented in Table 4. Starting with the comparison of Ni/ACs, the presence of larger particles in the AC_H and AC_Z supports (previously suggested on the basis of N_2 sorption data) was confirmed. Furthermore, the incorporation of ceria was found to be responsible for an important reduction of this parameter, in line with previous results on activated carbons for the Sabatier reaction.[36] Indeed, reductions of 67, 46, and 50% in the average Ni^0 particle sizes were found for the AC_H, AC_Z, and AC_C carbons, respectively, when adding ceria. Furthermore, ceria promotes the formation of better-dispersed nickel particles, and the particle size distribution reveals that cerium-containing samples tend to cluster within a narrower diameter range, resulting in a tighter curve (Figure 8). This indicates a higher number of particles with similar diameters compared to a non-cerium-doped catalyst, which exhibits a broader Gaussian distribution. Overall, while the smallest particles were found in Ni/AC_C (16 nm) among the Ni catalysts, similar sizes were found for NiCe/AC_H and NiCe/AC_C (7 and 8 nm, respectively) among the Ce-containing ones.

3.3. Catalytic Performances

Catalysts were tested under carbon dioxide methanation conditions, with CO_2 conversions and CH_4 yields being presented in Figure 9. For Ni/ACs, the results followed the trend: Ni/AC_C > Ni/AC_Z > Ni/AC_H. These results could be explained by (i) the basicity of the AC supports (pH_{PZC}: AC_C > AC_Z > AC_H), known as a favorable property for CO_2 methanation since it promotes CO_2 adsorption and stabilizes the intermediate species formed upon CO_2 activation;[7] (ii) the presence of impurities in the AC_Z and AC_H carbons which could potentially inactivate Ni; and (iii) the average nickel particle sizes in the catalysts: Ni/AC_Z (24 nm) > Ni/AC_H (21 nm) > Ni/AC_C (16 nm), taking into account that, for a fixed mass of catalyst, smaller Ni^0 particles provide a higher number of exposed metal sites available for the dissociative adsorption of H_2, with frequent positive consequences on the kinetics of the reaction and on the observed conversion. The relative importance of these factors may, however, change among the samples. In particular, Ni/AC_H exhibits smaller Ni particles than Ni/AC_Z but lower activity, which suggests that in the absence of a dedicated CO_2-activating phase, support basicity (together with the impurity content) plays a more decisive role than metal dispersion in this series.

Regarding NiCe/ACs, it is clear that the addition of ceria, responsible for a remarkable reduction in nickel particle sizes and known to be able to activate CO_2 molecules,[36,44,45] boosted the CO_2 methanation performance. Indeed, CH_4 yields higher than 50% were obtained for all NiCe/ACs above 305 °C, while none of the Ni/AC samples reached these values even at the highest tested temperature (450 °C). When comparing among catalysts, the results followed the trend: NiCe/AC_H = NiCe/AC_C > NiCe/AC_Z. Considering that the ceria loading was the same in all catalysts, its effect on the CO_2 adsorption capacity is expected to be similar in all samples.

https://doi.org/10.1021/acs.energyfuels.6c01629
Energy Fuels 2026, 40, 14787−14798

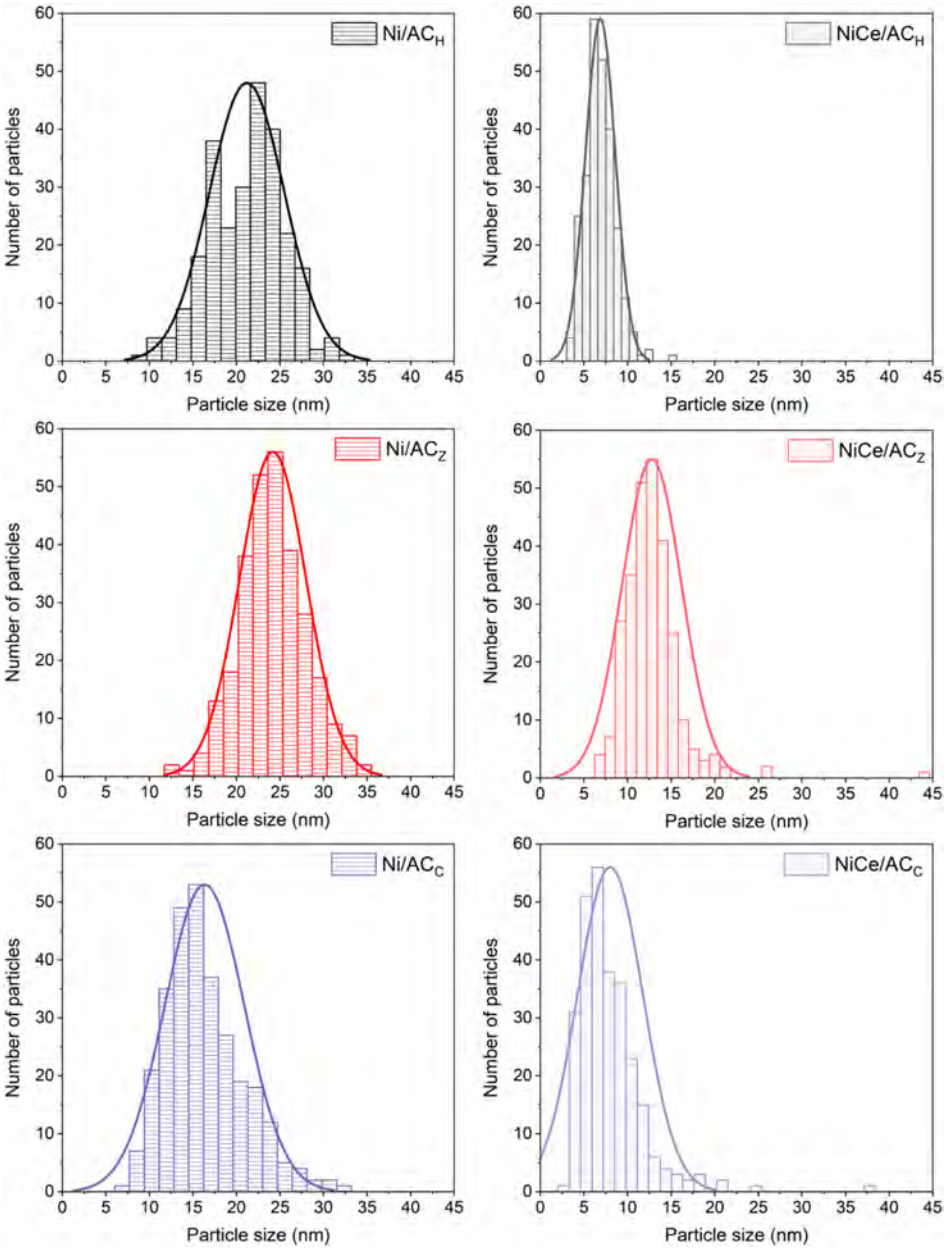

Figure 8. Histograms obtained for Ni and Ni−CeO_2-based activated carbons.

Thus, the almost coincident results from AC_H and AC_C-based NiCe catalysts could be ascribed to the average Ni^0 sizes in the samples (7 and 8 nm, respectively), significantly lower than that determined for NiCe/AC_Z (13 nm), which translates into a larger fraction of Ni^0 sites available for H_2 dissociation. In addition, as the NiCe/AC_Z hydrophobicity (h index = 0.82) was lower than that of NiCe/AC_C and NiCe/AC_H (h index = 0.91 in both cases), the potentially lower inhibitory role of water in the last two catalysts could also be behind their better performance. It should be pointed out that basicity played a more important role in the absence of effective active sites for carbon dioxide activation (CeO_2), while, once this functionality is guaranteed in the catalysts, their activity (remarkably higher) is more dependent on other factors such as water affinity and Ni^0 average particle size. All catalysts were analyzed by XRD after the tests, with the patterns being presented in Figure 4. As observed, no reoxidation of metallic nickel into NiO was identified, as shown by the absence of diffraction peaks attributed to this phase.

In the case of NiCe/AC_C, a longer catalytic test was run, with the results being presented in Figure 10. As observed, a 5% loss of CO_2 conversion (from 74% to 69% at ∼350 °C) and a 2% loss of CH_4 selectivity (from 99% to 97% at ∼350 °C) were registered after 43 h under reaction conditions. It should be pointed out that, after the step carried out at the lower reaction temperature (∼250 °C), the activity and selectivity at 350 °C were maintained. Furthermore, before and after the long-term experiment, a one-day test at variable temperatures was conducted on the same sample. The catalytic performance for these two tests can be seen in Figure 11 and shows that while the activity is similar in both tests above 350 °C, the long-term experiment had a greater impact on the performance at lower temperatures (300 to 350 °C). This indicates that the catalyst's properties might be affected by the experiment, potentially contributing to particle growth.

https://doi.org/10.1021/acs.energyfuels.6c01629
Energy Fuels 2026, 40, 14787−14798

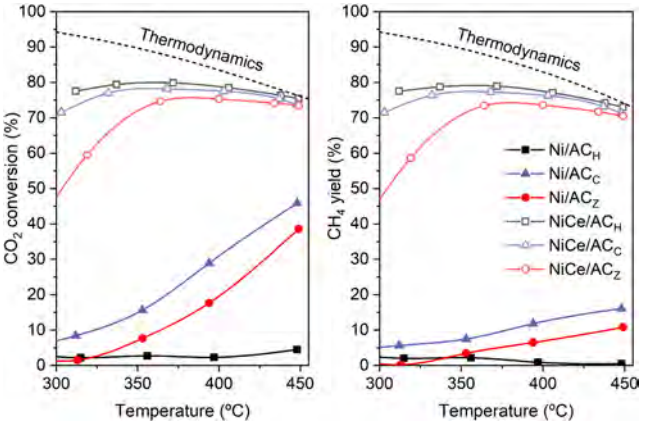

Figure 9. CO_2 conversions (left) and CH_4 yields (right) obtained for Ni- and Ni−CeO_2-based activated carbons. Conditions: atmospheric pressure, 86100 mL g_{cat}^{-1} h^{-1}, P_{CO2} = 0.16 bar, H_2:CO_2 = 4:1.

Regarding the comparison with the literature results (Table 5), NiCe/AC_H and NiCe/AC_C present similar or even better performance, especially considering the high activity and selectivity registered for these catalysts at a relatively low reaction temperature (310 °C). Worth pointing out is the study conducted by Li et al.,[46] who tested a commercial coconut shell (CSC)-derived activated carbon, chemically activated with HNO_3, and impregnated with Ni and different loadings of Mg as a promoter to obtain Ni/Mg ratios of 0.13, 0.26, and 0.39. The best results were achieved with the Ni−$Mg_{0.26}$/CSC catalyst, with the performance attributed to this material's higher basicity and smaller Ni^0 particle size (~18 nm). However, at temperatures between 300 and 350 °C, the NiCe/AC_C catalyst of the present work performs better in terms of CO_2 conversion (300 °C: 71% vs 20%; 350 °C: 78% vs 67%) and shows similar CH_4 selectivity (300 °C: 98% vs 96%; 350 °C: 99% vs 98%).

4. CONCLUSIONS

This work examines the effect of chemical (H_3PO_4 and $ZnCl_2$) and physical (CO_2) activation on coconut shell-derived carbons for use as catalyst supports in the Sabatier reaction. The findings show that chemical activation significantly enhances the S_{BET} surface area, attributed to a higher concentration of mesopores compared to the physically activated carbon. Additionally, a key difference between the activation methods is that CO_2-activated carbons are free from chemical contaminants and exhibit greater basicity (AC_C > AC_Z > AC_H), a crucial property for CO_2 activation during the methanation process. TGA experiments confirm that all activated carbons remain stable up to 500 °C, which falls within the operational temperature range of the Sabatier reaction. Monometallic and bimetallic catalysts were prepared via impregnation and coimpregnation, respectively, using the three activated carbons as supports. Ni incorporation had a stronger impact on the textural properties of the chemically activated carbons (AC_H and AC_Z), reducing the mesoporous volume and BET surface area, while AC_C remained largely unaffected (~0.06 cm^3 g^{-1} V_{meso}, ~500 m^2 g^{-1} S_{BET}). Compared to the monometallic catalysts, CeO_2 addition presents both benefits and challenges. It reduces the textural properties [S_{BET} (m^2 g^{-1}): AC_Z (902 to 487) > AC_C (531 to 322) > AC_H (763 to 281)], likely due to particle deposition inside the pores or on the catalyst surface, and decreases the hydrophobicity, with the hydrophobicity index dropping from 0.95−1 to 0.82−0.91, due to the higher affinity of CeO_2 for water molecules. However, CeO_2 also decreases the Ni^0 particle size by 67%, 46%, and 50% for AC_H, AC_Z, and AC_C, respectively, resulting in Ni^0 particles of 7, 13, and 8 nm, while improving the dispersion of Ni^0 active sites, as observed in the TEM analysis.

As a result, improved catalytic performance was observed for the bimetallic catalysts, with the highest CH_4 yield (~80% at 370 °C) achieved for the H_3PO_4 and CO_2-derived activated carbons. This demonstrates that the smaller Ni^0 particles, enhanced metallic dispersion, and the promotion of CO_2 activation on CeO_2 sites significantly boosted the catalytic activity. The AC_C catalyst was selected for evaluation under aging conditions in a 43-h test due to its optimal combination of greener preparation and high performance, demonstrating stability with no significant activity loss.

Compared with other Ni-supported catalysts in the literature, the coconut shell-derived activated carbons from

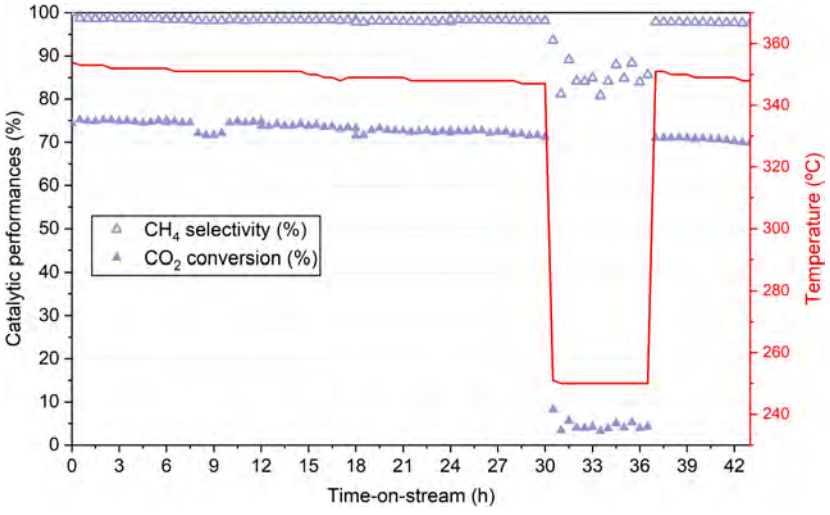

Figure 10. Catalytic performances obtained for NiCe/AC_C during a long-term experiment of 7 days (~6 h/day). Conditions: atmospheric pressure, 86100 mL g_{cat}^{-1} h^{-1}, P_{CO2} = 0.16 bar, H_2:CO_2 = 4:1.

https://doi.org/10.1021/acs.energyfuels.6c01629
Energy Fuels 2026, 40, 14787−14798

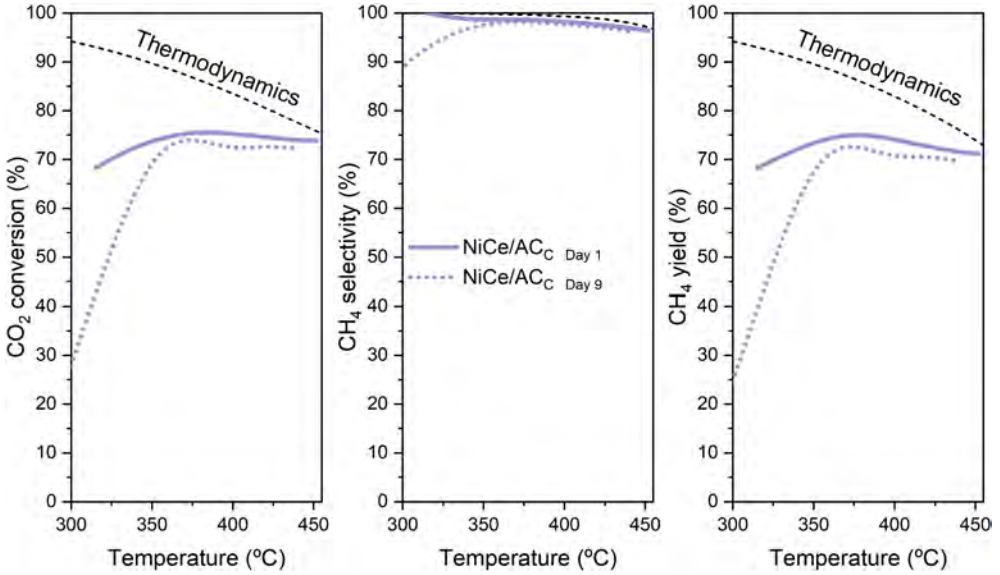

Figure 11. CO_2 conversions, CH_4 selectivity, and CH_4 yield obtained for $NiCe/AC_C$ before (day 1) and after (day 9) the long-term experiment. Conditions: atmospheric pressure, 86100 mL g_{cat}^{-1} h^{-1}, P_{CO2} = 0.16 bar, H_2:CO_2 = 4:1.

Table 5. Comparison of $NiCe/AC_H$ and $NiCe/AC_C$ Performances with Other Carbon-Supported and Ni−CeO_2 Systems from Literature

Catalyst	Q_T/W (ml g_{cat}^{-1} h^{-1})	Temperature (°C)	CO_2 conversion (%)	CH_4 selectivity (%)	Reference
$NiCe/AC_C$	86100	310	77	99	This work
$NiCe/AC_H$	86100	310	79	99	This work
Ru/CNF[a]	80000	500	52	100	47
Ni/CNT[b]	50000	340	51	96	48
Ni/N-CNT[c]	60000	360	88	99	49
NiCe/AC	16000	450	40	65	28
NiCe/AC	86100	360	70	99	36
NiCe/CNT	30000	350	84	100	50
NiCe/Kaolin	42000	350	59	98	51
NiCeZr/AC	40000	300	85	100	52
NiZr/CNT[b]	20000	400	55	96	53
NiMg/AC	10000	350	67	98	46
NiCe/SBA-15	86200	350	70	97	54
NiCe/MCM-41	86200	400	75	95	54
NiCe/FDU-12	60000	400	81	97	55
$NiCe/Al_2O_3$	15000	350	85	100	56
Ni/CeO_2	72000	300	87	100	57
NiCe/USY	86200	305	78	99	44

[a]Carbon nanofibers. [b]Carbon nanotubes. [c]Carbon nanotubes were doped with N.

the present study presented similar and/or better results, highlighting their potential for this reaction.

■ ASSOCIATED CONTENT

Supporting Information

The Supporting Information is available free of charge at https://pubs.acs.org/doi/10.1021/acs.energyfuels.6c01629.

SEM-EDS results by analyzed region for ACH, ACZ, and ACC activated carbons (Figure S1); TGA profiles obtained under nitrogen flow for ACH, nickel nitrate precursor salt, and uncalcined Ni/ACH catalyst (Figure S2); XRD patterns of ACH, ACZ, and ACC (Figure S3); isotherms (A) and pore size distribution (B) obtained for ACH, ACZ, and ACC (Figure S4); isotherms (A), pore size distribution (B), TEM micrographs (C), and histograms (D) obtained for ACH carbon loaded with 2 to 30 wt % Ni (Figure S5); main properties and best performances obtained for ACH carbon loaded with 2−30 wt % Ni (Table S1); pore size distributions obtained by BJH method for Ni and Ni−CeO_2-based ACs as well as for the corresponding supports (Figure S6); TEM micrographs obtained for ACH, ACZ, and ACC (Figure S7) (PDF)

■ AUTHOR INFORMATION

Corresponding Authors

Carmen Bacariza − *Centro de Química Estrutural, Institute of Molecular Sciences, Departamento de Engenharia Química, Instituto Superior Técnico, Universidade de Lisboa, Lisboa*

https://doi.org/10.1021/acs.energyfuels.6c01629
Energy Fuels 2026, 40, 14787−14798

1049 001, Portugal; orcid.org/0000-0003-4236-6724; Email: maria.rey@tecnico.ulisboa.pt

Stefania Specchia − *Politecnico di Torino, Department of Applied Science and Technology, Torino 10129, Italy;* orcid.org/0000-0003-3882-3240; Email: stefania.specchia@polito.it

Authors

Vittorio Vitacchione − *Politecnico di Torino, Department of Applied Science and Technology, Torino 10129, Italy*

Paula Teixeira − *Centro de Química Estrutural, Institute of Molecular Sciences, Departamento de Engenharia Química, Instituto Superior Técnico, Universidade de Lisboa, Lisboa 1049 001, Portugal;* orcid.org/0000-0002-6137-6664

José M. Lopes − *Centro de Química Estrutural, Institute of Molecular Sciences, Departamento de Engenharia Química, Instituto Superior Técnico, Universidade de Lisboa, Lisboa 1049 001, Portugal*

Carlos Henriques − *Centro de Química Estrutural, Institute of Molecular Sciences, Departamento de Engenharia Química, Instituto Superior Técnico, Universidade de Lisboa, Lisboa 1049 001, Portugal;* orcid.org/0000-0001-5878-5742

Complete contact information is available at: https://pubs.acs.org/10.1021/acs.energyfuels.6c01629

Notes

The authors declare no competing financial interest.
[§]Previous affiliation.

■ ACKNOWLEDGMENTS

The authors gratefully thank Professor Isabel Fonseca, Professor Maria Bernardo, and Professor Inês Matos from the *Faculdade de Ciências e Tecnologia* of the *Universidade Nova de Lisboa* for providing the activated carbons used in this study, as well as their corresponding pH_{PZC} values. The authors also acknowledge the financial support of the Portuguese Foundation for Science and Technology I.P. (FCT) through the following Research Projects: UIDB/00100/2020 (DOI: 10.54499/UIDB/00100/2020), UIDP/00100/2020 (DOI: 10.54499/UIDP/00100/2020), and LA/P/0056/2020 (DOI: 10.54499/LA/P/0056/2020). C.B. also thanks FCT for the contract 2020.00030.CEECIND (DOI: 10.54499/2020.00030.CEECIND/CP1587/CT0003).

■ REFERENCES

(1) Sun, C.; Da Costa, P. Transition Metal-Based Catalysts for CO2Methanation and Hydrogenation. In *Heterogeneous Catalysis*, Cesario, M. R.; de Macedo, D. A. eds., Elsevier; 2022, pp. 59−93. DOI: .

(2) Cui, Y.; He, S.; Yang, J.; Gao, R.; Hu, K.; Chen, X.; Xu, L.; Deng, C.; Lin, C.; Peng, S.; Zhang, C. Research Progress of Non-Noble Metal Catalysts for Carbon Dioxide Methanation. *Molecules* **2024**, *29* (2), 374.

(3) Memon, M.A.; Jiang, Y.; Hassan, M.A.; Ajmal, M.; Wang, H.; Liu, Y. Heterogeneous Catalysts for Carbon Dioxide Methanation: A View on Catalytic Performance. *Catalysts* **2023**, *13* (12), 1514.

(4) Usman, M.; Podila, S.; Alamoudi, M. A.; Al-Zahrani, A. A. Current Research Status and Future Perspective of Ni- and Ru-Based Catalysts for CO2Methanation. *Catalysts* **2025**, *15* (3), 203.

(5) Bacariza, M. C.; Graça, I.; Lopes, J. M.; Henriques, C. Tuning Zeolite Properties towards CO2Methanation: An Overview. *ChemCatChem* **2019**, *11* (10), 2388−2400.

(6) Ashok, J.; Pati, S.; Hongmanorom, P.; Tianxi, Z.; Junmei, C.; Kawi, S. A Review of Recent Catalyst Advances in CO2Methanation Processes. *Catal. Today* **2020**, *356*, 471.

(7) Bacariza, M. C.; Spataru, D.; Karam, L.; Lopes, J. M.; Henriques, C. Promising Catalytic Systems for CO2 Hydrogenation into CH4: A Review of Recent Studies. *Processes* **2020**, *8* (12), 1646.

(8) Busca, G.; Spennati, E.; Riani, P.; Garbarino, G. Looking for an Optimal Composition of Nickel-Based Catalysts for CO2Methanation. *Energies* **2023**, *16* (14), 5304.

(9) Usman, M.; Fareed, A. G.; Amin, M. A Bibliometric Analysis of CO2Methanation: Research Trends and Comprehension of Effective Catalysts. *J. Iran. Chem. Soc.* **2024**, *21* (5), 1185−1201.

(10) Medina, O. E.; Amell, A. A.; López, D.; Santamaría, A. Comprehensive Review of Nickel-Based Catalysts Advancements for CO2Methanation. *Renewable Sustainable Energy Rev.* **2025**, *207*, 114926.

(11) Du, J.; Gao, J.; Gu, F.; Zhuang, J.; Lu, B.; Jia, L.; Xu, G.; Liu, Q.; Su, F. A Strategy to Regenerate Coked and Sintered Ni/Al2O3 Catalyst for Methanation Reaction. *Int. J. Hydrogen Energy* **2018**, *43* (45), 20661−20670.

(12) Strucks, P.; Failing, L.; Kaluza, S. A Short Review on Ni-Catalyzed Methanation of CO2: Reaction Mechanism, Catalyst Deactivation, Dynamic Operation. *Chem. Ing. Technol.* **2021**, *93* (10), 1526−1536.

(13) Iwanow, M.; Gärtner, T.; Sieber, V.; König, B. Activated Carbon as Catalyst Support: Precursors, Preparation, Modification and Characterization. *Beilstein J. Org. Chem.* **2020**, *16* (1), 1188−1202.

(14) Adeleye, A. T.; Akande, A. A.; Odoh, C. K.; Philip, M.; Fidelis, T. T.; Amos, P. I.; Banjoko, O. O. Efficient Synthesis of Bio-Based Activated Carbon (AC) for Catalytic Systems: A Green and Sustainable Approach. *J. Ind. Eng. Chem.* **2021**, *96*, 59−75.

(15) Akpasi, S. O.; Isa, Y. M.; Monama, T. P.; Kiambi, S. L.; Ngema, P. T. CO2Methanation: A Bibliometric Analysis and Review of Activated Carbon-Based Materials (2014−24). *Clean Energy* **2024**, *8* (6), 148−174.

(16) Gamal, A.; Jlassi, K.; Ahmad, Y. H.; Tang, M.; Al-Qaradawi, S. Y.; Chehimi, M. M.; Ozoemena, K. I.; Abdullah, A. M. Carbon-Supported Catalysts for Carbon Dioxide Methanation: A Review. *J. CO2 Util.* **2024**, *85*, 102881.

(17) Sun, Y.; Huo, K.; Fang, H.; Wang, Y.; Wu, M. A Review of Recent Progress on CO2 Hydrogenation to Methane by Ni-Based Catalysts Supported on Carbon Materials. *New Carbon Mater.* **2025**, *40* (6), 1201−1218.

(18) Lv, C.; Xu, L.; Chen, M.; Cui, Y.; Wen, X.; Li, Y.; Wu, C.; Yang, B.; Miao, Z.; Hu, X.; Shou, Q. Recent Progresses in Constructing the Highly Efficient Ni Based Catalysts With Advanced Low-Temperature Activity Toward CO2Methanation. *Front. Chem.* **2020**, *8*, 269.

(19) Heidarinejad, Z.; Dehghani, M. H.; Heidari, M.; Javedan, G.; Ali, I.; Sillanpää, M. Methods for Preparation and Activation of Activated Carbon: A Review. *Environ. Chem. Lett.* **2020**, *18* (2), 393−415.

(20) Abuelnoor, N.; AlHajaj, A.; Khaleel, M.; Vega, L. F.; Abu-Zahra, M. R. M. Activated Carbons from Biomass-Based Sources for CO2 Capture Applications. *Chemosphere* **2021**, *282*, 131111.

(21) Ha, N. N.; Ha, N. T. T.; Van Khu, L.; Cam, L. M. Theoretical Study of Carbon Dioxide Activation by Metals (Co, Cu, Ni) Supported on Activated Carbon. *J. Mol. Model.* **2015**, *21* (12), 322.

(22) Li, Y.; Li, D.; Rao, Y.; Zhao, X.; Wu, M. Superior CO2, CH4, and H2 Uptakes over Ultrahigh-Surface-Area Carbon Spheres Prepared from Sustainable Biomass-Derived Char by CO2 Activation. *Carbon* **2016**, *105*, 454−462.

(23) Völs, P.; Störr, B.; Lißner, A.; Mertens, F. A Comparative Study on the Influence of Potential 4th Period Promoters in Ni-Bimetallic Catalysts for CO2Methanation. *Fuel* **2024**, *358*, 130141.

(24) Nieß, S.; Armbruster, U.; Dietrich, S.; Klemm, M. Recent Advances in Catalysis for Methanation of CO2 from Biogas. *Catalysts* **2022**, *12* (4), 374.

(25) Qiao, Y.; Wu, C. Nitrogen Enriched Biochar Used as CO2 Adsorbents: A Brief Review. *Carbon Capture Sci. Technol.* **2022**, *2*, 100018.
(26) Wang, X.; Liu, Y.; Zhu, L.; Li, Y.; Wang, K.; Qiu, K.; Tippayawong, N.; Aggarangsi, P.; Reubroycharoen, P.; Wang, S. Biomass Derived N-Doped Biochar as Efficient Catalyst Supports for CO2Methanation. *J. CO2 Util.* **2019**, *34*, 733−741.
(27) Gonçalves, L. P. L.; Mielby, J.; Soares, O. S. G. P.; Sousa, J. P. S.; Petrovykh, D. Y.; Lebedev, O. I.; Pereira, M. F. R.; Kegnæs, S.; Kolen'ko, Y. V. *In Situ* Investigation of the CO2Methanation on Carbon/Ceria-Supported Ni Catalysts Using Modulation-Excitation DRIFTS. *Appl. Catal., B* **2022**, *312*, 121376.
(28) Di Stasi, C.; Renda, S.; Greco, G.; González, B.; Palma, V.; Manyà, J.J. Wheat-Straw-Derived Activated Biochar as a Renewable Support of Ni-CeO2 Catalysts for CO2 Methanation. *Sustainability* **2021**, *13* (16), 8939.
(29) Huang, B.; Li, W.; Shi, Z.; Yang, L.; Wen, Z.; Zi, G.; Luo, L. Effect of ZnCl2, H3PO4, and KOH Activation on Low-Temperature NH3-Denitration Performance of Activated Carbon. *CLEAN − Soil Air Water* **2024**, *52* (1), 2300148.
(30) Neme, I.; Gonfa, G.; Masi, C. Activated Carbon from Biomass Precursors Using Phosphoric Acid: A Review. *Heliyon* **2022**, *8* (12), No. e11940.
(31) Bandani, M.; Najafi, M.; Khalili, S.; Jahanshahi, M.; Peyravi, M.; Salmani, H. Preparation and Characterization of Low-Cost Chemically Activated Carbons Using H3PO4, ZnCl2 and KOH for CO2 Adsorption Applications. *Sci. Rep.* **2026**, *16* (1), 6288.
(32) Sathishkumar, R.; Prakash, R. A Review on Activated Carbons (AC) for CO2 Capture Applications: Preparation, Characterisation and Surface Modification Methods. *Fuel* **2026**, *405*, 136521.
(33) Bacariza, M. C.; Graça, I.; Lopes, J. M.; Henriques, C. Enhanced Activity of CO2 Hydrogenation to CH4 over Ni Based Zeolites through the Optimization of the Si/Al Ratio. *Microporous Mesoporous Mater.* **2018**, *267*, 9−19.
(34) Bacariza, M. C.; Maleval, M.; Graça, I.; Lopes, J. M.; Henriques, C. Power-to-Methane over Ni/Zeolites: Influence of the Framework Type. *Microporous Mesoporous Mater.* **2019**, *274*, 102−112.
(35) Bacariza, M. C.; Graça, I.; Westermann, A.; Ribeiro, M. F.; Lopes, J. M.; Henriques, C. CO2 Hydrogenation Over Ni-Based Zeolites: Effect of Catalysts Preparation and Pre-Reduction Conditions on Methanation Performance. *Top. Catal.* **2016**, *59* (2−4), 314−325.
(36) Mateus, F.; Teixeira, P.; Lopes, J. M.; Henriques, C.; Bacariza, C. CO2Methanation on Ni Catalysts Supported over Activated Carbons Derived from Cork Waste. *Energy Fuels* **2023**, *37* (12), 8552−8562.
(37) Satheesh, M.; Pugazhvadivu, M.; Prabu, B.; Gunasegaran, V.; Manikandan, A. Synthesis and Characterization of Coconut Shell Ash. *J. Nanosci. Nanotechnol.* **2019**, *19* (7), 4123−4128.
(38) Anuar, M. F.; Fen, Y. W.; Zaid, M. H. M.; Matori, K. A.; Khaidir, R. E. M. Synthesis and Structural Properties of Coconut Husk as Potential Silica Source. *Results Phys.* **2018**, *11*, 1−4.
(39) Carbon *Facts, Uses, & Properties*; Britannica. https://www.britannica.com/science/carbon-chemical-element.
(40) Omri, A.; Benzina, M. Characterization Of Activated Carbon Prepared From A New Raw Lignocellulosic Material: Ziziphus Spina-christi Seeds. *J. Soc. Chim. Tunis* **2012**, *14*, 175−183.
(41) Pelicano, C. M.; Rapadas, N. J.; Magdaluyo, E. X-Ray Peak Profile Analysis of Zinc Oxide Nanoparticles Formed by Simple Precipitation Method. *AIP Conf Proc.* **2017**, *1901* (1), 020016.
(42) Ullah, I.; Ahmed, S. M.; Lou, H.; Abbasi, Z.; Ahmad, Z.; Usman, M.; Wu, W.; Wang, Z. Boosting Low-Temperature CO2Methanation through Ni/ZrO2 Catalyst-NaA Zeolite Interplay. *J. Environ. Chem. Eng.* **2026**, *14*, 123407.
(43) Quindimil, A.; Onrubia-Calvo, J. A.; Davó-Quiñonero, A.; Bermejo-López, A.; Bailón-García, E.; Pereda-Ayo, B.; Lozano-Castelló, D.; González-Marcos, J. A.; Bueno-López, A.; González-Velasco, J. R. Intrinsic Kinetics of CO2Methanation on Low-Loaded Ni/Al2O3 Catalyst: Mechanism, Model Discrimination and Parameter Estimation. *J. CO2 Util.* **2022**, *57*, 101888.
(44) Bacariza, M. C.; Graça, I.; Lopes, J. M.; Henriques, C. Ni-Ce/Zeolites for CO2 Hydrogenation to CH4: Effect of the Metal Incorporation Order. *ChemCatChem* **2018**, *10* (13), 2773−2781.
(45) Westermann, A.; Azambre, B.; Bacariza, M. C.; Graça, I.; Ribeiro, M. F.; Lopes, J. M.; Henriques, C. The Promoting Effect of Ce in the CO2Methanation Performances on NiUSY Zeolite: A FTIR In Situ/Operando Study. *Catal. Today* **2017**, *283* (Supplement C), 74−81.
(46) Li, X.; Wang, Y.; Zhang, G.; Sun, W.; Bai, Y.; Zheng, L.; Han, X.; Wu, L. Influence of Mg-Promoted Ni-Based Catalyst Supported on Coconut Shell Carbon for CO2Methanation. *ChemistrySelect* **2019**, *4* (3), 838−845.
(47) Jiménez, V.; Sánchez, P.; Panagiotopoulou, P.; Valverde, J. L.; Romero, A. Methanation of CO, CO2 and Selective Methanation of CO, in Mixtures of CO and CO2, over Ruthenium Carbon Nanofibers Catalysts. *Appl. Catal. Gen.* **2010**, *390* (1), 35−44.
(48) Gödde, J.; Merko, M.; Xia, W.; Muhler, M. Nickel Nanoparticles Supported on Nitrogen−Doped Carbon Nanotubes Are a Highly Active, Selective and Stable CO2Methanation Catalyst. *J. Energy Chem.* **2021**, *54*, 323−331.
(49) Wang, W.; Duong-Viet, C.; Ba, H.; Baaziz, W.; Tuci, G.; Caporali, S.; Nguyen-Dinh, L.; Ersen, O.; Giambastiani, G.; Pham-Huu, C. Nickel Nanoparticles Decorated Nitrogen-Doped Carbon Nanotubes (Ni/N-CNT); a Robust Catalyst for the Efficient and Selective CO2Methanation. *ACS Appl. Energy Mater.* **2019**, *2* (2), 1111−1120.
(50) Wang, W.; Chu, W.; Wang, N.; Yang, W.; Jiang, C. Mesoporous Nickel Catalyst Supported on Multi-Walled Carbon Nanotubes for Carbon Dioxide Methanation. *Int. J. Hydrogen Energy* **2016**, *41* (2), 967−975.
(51) Aimdate, K.; Srifa, A.; Koo-Amornpattana, W.; Sakdaronnarong, C.; Klysubun, W.; Kiatphuengporn, S.; Assabumrungrat, S.; Wongsakulphasatch, S.; Kaveevivitchai, W.; Sudoh, M.; Watanabe, R.; Fukuhara, C.; Ratchahat, S. Natural Kaolin-Based Ni Catalysts for CO2Methanation: On the Effect of Ce Enhancement and Microwave-Assisted Hydrothermal Synthesis. *ACS Omega* **2021**, *6* (21), 13779−13794.
(52) Le, M. C.; Le Van, K.; Nguyen, T. H. T.; Nguyen, N. H. The Impact of Ce-Zr Addition on Nickel Dispersion and Catalytic Behavior for CO2Methanation of Ni/AC Catalyst at Low Temperature. *J. Chem.* **2017**, *2017*, 4361056.
(53) Romero-Sáez, M.; Dongil, A. B.; Benito, N.; Espinoza-González, R.; Escalona, N.; Gracia, F. CO2Methanation over Nickel-ZrO2 Catalyst Supported on Carbon Nanotubes: A Comparison between Two Impregnation Strategies. *Appl. Catal., B* **2018**, *237*, 817−825.
(54) Bacariza, M. C.; Graça, I.; Bebiano, S. S.; Lopes, J. M.; Henriques, C. Micro- and Mesoporous Supports for CO2Methanation Catalysts: A Comparison between SBA-15, MCM-41 and USY Zeolite. *Chem. Eng. Sci.* **2018**, *175* (Supplement C), 72−83.
(55) Liu, Q.; Dong, H. In Situ Immobilizing Ni Nanoparticles to FDU-12 via Trehalose with Fine Size and Location Control for CO2Methanation. *ACS Sustain. Chem. Eng.* **2020**, *8* (4), 2093−2105.
(56) Liu, H.; Zou, X.; Wang, X.; Lu, X.; Ding, W. Effect of CeO2 Addition on Ni/Al2O3 Catalysts for Methanation of Carbon Dioxide with Hydrogen. *J. Nat. Gas. Chem.* **2012**, *21* (6), 703−707.
(57) Atzori, L.; Cutrufello, M. G.; Meloni, D.; Cannas, C.; Gazzoli, D.; Monaci, R.; Sini, M. F.; Rombi, E. Highly Active NiO-CeO2 Catalysts for Synthetic Natural Gas Production by CO2Methanation. *Catal. Today* **2018**, *299*, 183−192.